TECHNICAL PAPER

Multi-objective genetic algorithm (MOGA) based optimization of high-pressure coolant assisted hard turning of 42CrMo4 steel

Shanta Saha[1] · Prianka B. Zaman[2] · Md. Imran Hasan Tusar[3] · Nikhil R. Dhar[2]

Abstract

This study aims at finding a set of optimum solutions of cutting conditions for the machining responses of cutting temperature and surface roughness in hard turning of 42CrMo4 alloy steel at high-pressure coolant (HPC) condition. Comparative experimental investigations between dry and HPC cutting environments were performed to evaluate the stated responses concerning the factors of cutting speed, feed, and work-piece hardness. The full factorial method was employed for the experimental design. The measured value of cutting temperature and surface roughness was found in a reduced amount for HPC condition compared to dry cut for all of the machining runs. Empirical models were developed by response surface methodology for the responses of HPC-assisted machining. The ANOVA result indicated that cutting speed and hardness has the greatest effect on cutting temperature and surface roughness, respectively. Design of experiment (DoE) based optimization was carried out that results in the best optimum settings of 147 m/min cutting speed, 0.12 mm/rev feed rate and 42HRC work-piece hardness. Genetic algorithm based multi-objective optimization was then performed that simultaneously minimizes both of the response models. Within the constraints of experimental design, the optimal set resulted at the range of 86–165 m/min cutting speed, 0.12–0.13 mm/rev feed rate and HRC 42–44 work-piece hardness.

Keywords Hard turning · High-pressure coolant · RSM · MOGA · Cutting temperature · Surface roughness

1 Introduction

Machining of hardened material with hardness generally between 40 to 60HRC by a single-point cutting tool is called the hard turning process [1, 2]. This process is considered as the replacement of grinding operations due to its benefits of cost reduction and higher productivity [3]. Despite this, hard turning possesses some machining complexity in achieving a superior surface quality than grinding operation. It is recognized that an insert with a negative rake angle is required for hard turning to avoid tool breakage [4]. However, the incorporation of a large negative rake angle produces more compressive force. This leads to a significant amount of heat generation which contributes adversely to machining performance in terms of poor part quality [5]. Again, the martensitic layer can be generated in the part due to rapid cooling and heating, causing compressive residual stress [6]. If the material under compressive stress exceeds the yield strength, the tensile residual stress occurs after cooling [7] and may cause premature failure of the machined part [8, 9]. These negative consequences of hard turning are associated with the metallurgical effect depending on the cooling rate as well as cutting temperature [10]. So that, during hard turning, it is essential to provide an effective coolant application method that can eventually lessen the cutting temperature and give a better surface finish.

Considering the cutting environment, the conventional fluid application does not always extensively assist in limiting the temperature, especially for high speed and hard machining [11]. At this point, the high-pressure coolant (HPC) application technique gives a better solution. Coolant injection at high pressure functionally infiltrates into the cutting zone and eradicates heat before its accumulation [12]. This integrity of HPC over conventional fluid applications was

✉ Prianka B. Zaman
  prianka@ipe.buet.ac.bd

[1] Department of Industrial and Production Engineering, Shahjalal University of Science and Technology, Sylhet 3114, Bangladesh

[2] Department of Industrial and Production Engineering, Bangladesh University of Engineering and Technology, Dhaka 1000, Bangladesh

[3] Department of Mechanical and Industrial Engineering, Louisiana State University, Baton Rouge, USA

thoroughly examined across the years by several researchers. The studies support that, machining under HPC provides better chip control, superior component quality, enhanced tool life and higher cutting parameters to choose [13–18]. Besides, the HPC injection technique also decreases the consumption of cutting fluid by two to four times [11, 19].

To get a useful insight into the mechanics of cutting effect on responses, various empirical modeling approach was adopted. Besides the effective investigation of different input parameters, various single or multi-objective approaches were also implemented by many authors to confirm that these parameters yield the desired responses. Taguchi L27 was applied by Rao et al. [20] for the turning trials of AISI 1050 steel for cutting force and surface roughness evaluation. Singla and Singh [21] studied the effects of various machining parameters on the surface roughness and material removal rate (MRR) in the hard turning of vanadium steel. They utilized Taguchi L9 orthogonal array for the design of the experiment. S/N ratio and ANOVA were used to study the outcomes. Ozel et al. [22] developed a model using regression analysis and Artificial Neural Network (ANN) for the prediction of surface finish and flank wear in finish turning of AISI D2 steels (60HRC). Suresh and Basavarajappa [23] used response surface methodology (RSM) to study the consequence of various cutting parameters in hard turning of AISI H13 steel with PVD coated TiCN ceramic tool. They developed models for tool wear and surface roughness. RSM was also used for a force prediction model in hard turning of AISI 52,100 steel (60HRC) using the CBN tool [24]. Cutting forces generated from turning of AISI 1045 with tungsten carbide tool was investigated by RSM coupled with factorial design [25]. RSM and ANN were employed by Mia and Dhar [26] to predict the average tool-work-piece interface temperature in hard turning of AISI 1060. Zahia et al. [27] applied RSM to determine optimum cutting conditions with the goal of lower surface roughness and cutting force. They studied AISI 4140 alloy steel (56HRC) that was machined with PVD coated ceramic insert.

RSM or Taguchi, such type of multi-objective optimization base techniques mostly are priori base which eventually makes the problem single objective [28]. However, the success of optimization in the complex nature of machining is inherent in considering several objectives ensuing a non-dominated solution set. In the hard turning process, the application of multi-objective optimization coming with the non-dominated optimal solution is targeted to apply in this study. To optimize the machining parameters with multi-goals, different techniques such as statistical, finite element method, artificial intelligence (AI) method, etc. were employed by many researchers [29–32]. AI methods for multi-goals that are finding their way to the machining process optimization field include Genetic algorithms (GA) [33], ANN [34], Particle Swarm Optimization [35], Bees

Algorithm [36], Artificial Bee Colony [37] and Differential Evolution [38]. Among these, GA is known as a popular meta-heuristic algorithm that is mostly compatible with the multifaceted problem like machining [33]. Further, GAs are customized to promote solution diversity; i.e. it holds the property of not getting stuck in local optima. Over that, in the perspective of multi-objective optimization, the resolving technique of multi-objective genetic algorithm (MOGA) uses a controlled elitist GA. This contributes in diversity creation of the population even holding a lower fitness value and offers Pareto optimal set [39]. Researchers applied this MOGA approach at several machining processes for several process parameter optimization [40–43].

RSM is a popular method for modeling purposes and GA is considered an effective technique for multi-objective optimization to build a non-dominated solution set. To the best of the author's knowledge, optimization of cutting temperature and surface roughness simultaneously with the MOGA approach was not applied for hard machining of 42CrMo4 alloy steel with coated carbide insert. On the other hand, most of the studied hard turning based researches were performed under dry or near-dry environment and the study on the optimization through the MOGA approach for the hard turning of the stated tool-work pair under HPC was not found. It can also be inferred that the responses of hard turning operation were typically studied for different ranges of machining parameters for the material with the same hardness. Hence, another target of this study is to differ the work-piece hardness along with cutting speed and feed variation. Therefore, the purpose of the current study is a hard turning of 42CrMo4 alloy steel by coated carbide insert under HPC and then optimizing the responses—cutting temperature and surface roughness in terms of the variables—cutting speed, feed rate, and material hardness. Experimental studies include the performance evaluation of HPC machining compared to dry cut in terms of these responses and the effective investigation of the variables while machining with HPC jet. The experimental results at the HPC condition are used to develop the response predictive models based on RSM. Finally, the models have been used as minimization objective functions for multi-objective optimization.

2 Experimental methodology

2.1 Work-piece and cutting tool

Machining experiments were carried out on alloy steel 42CrMo4 in the form of a 98 mm diameter shaft with a cut length of 200 mm. Three shafts of this dimension were machined while material hardness was varied at three levels. The cutting insert with a general specification of SNMM 120,408 (WIDIA) was used as a cutting tool that

Table 1 Control parameters with their levels

Parameters	Unit	Levels			
Cutting speed (V)	m/min	54	82	118	165
Feed rate (f)	mm/rev	0.12	0.14	0.16	–
Workpiece hardness (H)	HRC	42	48	56	–
Depth of cut (d)	mm	1.5	–	–	–
Environment	–	Dry	HPC	–	–

was mounted on a tool holder of designation PSBNR 2525 M12 (Sandvik). The insert was coated with TiCN, WC and Co with a tool geometry of -6°, -6°, 6°, 6°, 15°, 75°, 0.8 mm.

2.2 Experimental design

The experimental plan was associated with the straight turning of hardened steel of different hardness (42, 48 and 56HRC) under dry and high-pressure coolant environments. The ranges of cutting speed, V (54, 82, 118 and 165 m/min) and feed rate, f (0.12, 0.14 and 0.16 mm/rev) were selected based on the tool manufacturer's recommendation and industrial practices. The depth of cut (d) was kept fixed. The recommended range of depth of cut is 0.3 mm to 2 mm (WidiaTM Value) for the finishing operation of the studied tool-work-piece combination. Nevertheless, d should be greater than the nose radius of the insert. So, considering the entire facts d value was set to 1.5 mm which is greater than the nose radius of 0.8 mm and the approximate average value of the suggested range. The employed levels of input parameters along with their levels are summarized in Table 1. A mixed-level full factorial experimental design was applied for the selected levels of input variables. Thus, 36 $(3^2, 4^1)$ experimental series were formed for each of the cutting environments. Table 2 shows the resulting experimental design with corresponding measured responses.

2.3 Experimental set-up and response measurement

The straight turning operations were performed on a relatively rigid and powered center lathe (spindle power 7.5 kW, China). The coolant delivery system was utilized for continuous supplying of VG-68 (ISO grade) oil at high pressure from the coolant tank and aimed at the cutting region through the nozzle. Getting the positioning of the nozzle just right to the cutting zone is one of the keys to the effectiveness of this coolant delivery technology. A specially designed nozzle system developed by Khan [44] was incorporated into this coolant delivery arrangement. This nozzle tool consists of two outlet channels to impinge the pressurized coolant at a time at the rake and flank face of the cutting tool, respectively. Every channel diameter was 0.5 mm. The coolant flow

Table 2 Experimental design and results

Exp. no	Control parameters			Measured responses			
	V (m/min)	F (mm)	H (HRC)	T (°C)		R_a (μm)	
				Dry	HPC	Dry	HPC
1	54	0.12	42	328	107	1.52	0.98
2	82	0.12	42	361	116	1.30	0.85
3	118	0.12	42	416	131	1.04	0.75
4	165	0.12	42	449	165	0.94	0.72
5	54	0.14	42	377	120	1.88	1.00
6	82	0.14	42	394	132	1.50	0.90
7	118	0.14	42	437	147	1.20	0.78
8	165	0.14	42	514	174	1.14	0.74
9	54	0.16	42	405	138	2.08	1.02
10	82	0.16	42	449	154	1.80	0.98
11	118	0.16	42	487	176	1.50	0.84
12	165	0.16	42	568	230	1.32	0.78
13	54	0.12	48	380	111	1.70	1.00
14	82	0.12	48	399	130	1.40	0.91
15	118	0.12	48	420	165	1.10	0.79
16	165	0.12	48	459	209	0.98	0.74
17	54	0.14	48	403	132	2.00	1.01
18	82	0.14	48	421	148	1.60	0.94
19	118	0.14	48	463	175	1.40	0.79
20	165	0.14	48	529	264	1.33	0.75
21	54	0.16	48	426	143	2.40	1.04
22	82	0.16	48	459	175	2.00	1.00
23	118	0.16	48	502	220	1.70	0.88
24	165	0.16	48	626	345	1.50	0.80
25	54	0.12	56	415	131	1.85	1.20
26	82	0.12	56	437	148	1.60	1.14
27	118	0.12	56	503	174	1.45	1.07
28	165	0.12	56	546	225	1.28	0.99
29	54	0.14	56	426	145	2.17	1.27
30	82	0.14	56	481	176	1.82	1.24
31	118	0.14	56	524	220	1.56	1.14
32	165	0.14	56	590	296	1.49	1.02
33	54	0.16	56	492	165	2.60	1.32
34	82	0.16	56	546	187	2.22	1.30
35	118	0.16	56	633	238	1.80	1.22
36	165	0.16	56	700	407	1.60	1.10

rate through each channel was 6 l/min at the pressure of 8 MPa. The pictorial view of the experimental setup is shown in Fig. 1.

As the machining performance; two response factors—cutting temperature (T) and surface roughness (R_a) were considered and measured by specific instruments. T was quantified through the tool-work thermocouple technique. The calibration for this tool-work pair was used for convert-

Fig. 1 Photographic view of the experimental set-up
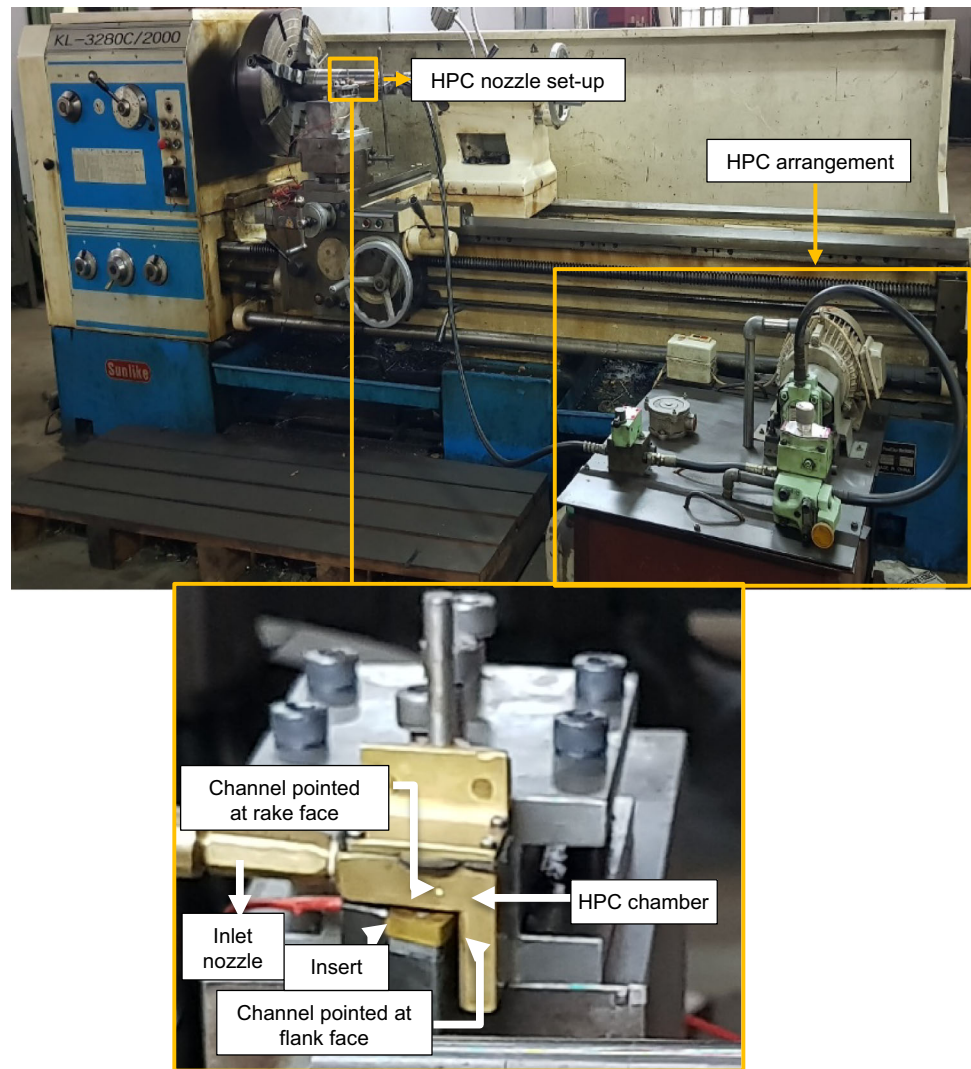
ing emf (mV) to temperature (°C) while the emf generated by this was recorded by a digital multimeter (Rish Multi, India). R_a measurement was performed by a contact-type surface roughness tester named Talysurf (Surtronic 3 +) with a 0.8 mm sampling length. This measurement was repeated three times at several places of the workpiece, and the mean value was incorporated in the study. The cutting tool insert was changed every four-machining to reduce the tool wear effect on the performance. Within consecutive three days, all of the experiments were completed so that, weather effect is seemed to be negligible to the responses. To ensure the reliability of the results and to minimize the effect of machine uncontrollable factors each of the experiments was performed two times. After all, the average value of each measured response was calculated and employed for the analysis. The average values of the responses are presented in Table 2.

3 Mathematical model development

Response Surface Methodology (RSM) of the Design-Expert Software V7.0 was used to construct the mathematical models in this study. The mathematical model used in RSM is typically a first or second-order polynomial model based on regression analysis. The first-order model follows as Eq. (1), which includes only the main effects of the variable. In this equation, Y is the response variable of the system, and ε is the normally distributed dependent variable.

$$Y = b_0 + \sum_{i=1}^{k} b_i x_i + \varepsilon \tag{1}$$

While the curvature in the true response surface is strong enough that the interaction of variables is there, a second-order model is likely to be required. Equation (2) indicates

the general second-order model where, $b_{ij} = 0, 1, 2..., k$ are the regression coefficients.

$$Y = b_0 + \sum_{i=1}^{k} b_i x_i + \sum_{i=1}^{k} b_{ii} x_i^2$$
$$+ \sum_{i<j} \sum_{j=2}^{k} b_{ii} x_i x_j + \varepsilon \qquad (2)$$

In this study, a historical data-dependent experimental design was employed in modeling. The models relate the selected parameters-cutting speed, feed rate, and work-piece hardness to each of the responses—cutting temperature and surface roughness for HPC cutting condition. Accordingly, various statistical validity tests were performed to check the acceptability of the developed models.

4 Genetic algorithm (GA) based multi-objective optimization

The optimization model formulated in the present work is a bounded constraint multi-objective optimization problem solved by real-valued GA named continuous GA. Compared to binary, continuous GA is faster and requires less storage. GA is considered as natural selection and natural genetics-based search algorithms. The procedure is generative and starts with a random 'initial population'. The double vector type population was selected for the present problem as this is the mixed-integer program. A fitness function $F(x)$ is first derived from the objective function $f(x)$ and used in successive genetic operations. The population is comprised of a group of chromosomes that are developed through several consecutive iterations. For the production of offspring each of the populations is evaluated and then selected according to the fitness value. The offspring are then inserted into the population replacing the parents, producing a new generation. The new population is further evaluated and tested for termination. This whole process of GA encompasses three leading operators- selection, crossover, and mutation.

4.1 Selection

The selection operator selects the fittest candidate from the current generation. It selects good strings in a population and forms a mating pool with a probability proportional to the fitness (F_i). Since, population size is usually kept fixed in simple GA, the sum of the probability (p_i) of the strings being selected for the mating pool must be 1. p_i of selecting the ith string is given in the following equation-
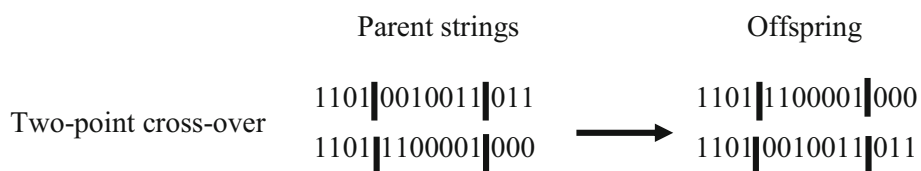
$$p_i = \frac{F_i}{\sum F_j}$$

where, i and j vary from 1 to n, n being the population size.

Among many of the selection mechanisms, roulette wheel selection (RWS) and tournament selection (TS) is favorable to many researchers. As RWS cannot handle negative fitness values and a minimization problem directly [45]; TS is chosen to apply in this study. TS can handle either minimization or maximization problems and minimize the early convergence of the algorithm [46]. TS involves running several tournaments among a few individuals at random. If the tournament size is larger, weak individuals have a smaller chance to be selected. In each tournament, the individual with the best fitness is selected for crossover.

4.2 Crossover

Parents are recombined by a crossover operator to produce new solutions called offspring. New strings are created by exchanging information among strings of the mating pool. In most of the crossover operators, two strings are picked from the mating pool at random and some portions of the strings are exchanged between the strings. The crossover operator is divided in many ways such as single point, two-point, uniform, arithmetic, etc. Due to the ability to operate on any chromosome representation, the two-point crossover was used here. This crossover process is shown as follows:

	Parent strings	Offspring
Two-point cross-over	1101|0010011|011 1101|1100001|000	1101|1100001|000 1101|0010011|011

The vertical line indicates the chosen crossover point. If good strings are created by crossover there will be more copies of them in the next mating pool generated by the reproduction operator. But if good strings are not created by crossover, they will not survive too long. Thus, the crossover operator is not applied to all parents but it is applied with probability which is normally set equal to 0.6 to 0.95 [42]. Here, the crossover was performed, with the chosen crossover rate of 0.8.

4.3 Mutation

The mutation operator is used to maintain genetic diversity from one generation of a population to the next. Thus, mutation provides diversity in the population and enables the GA to search a broader space. This operator randomly changes 1 to 0 and vice-versa with a small probability, normally 0.001 and 0.01 [47]. With non-binary representations, the mutation is achieved by either perturbing the gene values or random selection of new values within the allowed range. Here, as the problem is constraint associated, the 'adaptive feasible' type of mutation was used. This function randomly generates directions that are adaptive concerning the last successful or unsuccessful generation. The mutation chooses a direction and steps length that satisfies bounds and linear constraints.

These successive operators are repeated for several generations to get the best solution or solution set. But, there is no distinct way of recognizing how large this number should be. Here, ANOVA is performed on several GA runs while the number of generations is varied. The highest number of generations with no differences in means with compared one is selected for the final GA run.

The ultimate goal of MOGA is to identify solutions in the Pareto optimal set. The expression of a general multi-objective design problem for minimization is following:

$$\min F(x) = (f_1(x), f_2(x), \ldots, f_k(x))$$
$$s.t.\ x \in S$$
$$x = (x_1, x_2, \ldots, x_n)$$

where, $f_1(x), f_2(x), \ldots, f_k(x)$ are the k objectives functions, $x_1, x_2, \ldots, x_n$ are the n optimization parameters, and $S \epsilon R^n$ is the solution space.

In this study, the fitness value was used to compute the next generation from the randomly generated initial population. To control the superiority of GA for MOGA, 'Pareto Fraction' and 'Distance Fcn' were used. The former confines the number of individuals on the Pareto front. While the latter maintains the diversity by favoring individuals that are relatively far away from others holding the same rank on the front. 'Phenotype' is used as the crowding-distance function that calculates the distance and creates the diversity in function space. By default, the solver tries to limit the number of

individuals to 35% (Pareto fraction) of the population size. The solver stops when any one of the three criteria is met. The first criterion is the maximum number of generations. The second one is—if the average change in the spread of the Pareto front over the 'Max Stall Generations' (default is 100) is less than the specified tolerance (default is $1e^{-4}$). The last condition is the maximum time limit (default is infinite). Two performance measures—average distance and spread were used for numerical comparison of the non-dominated fronts. These measures with smaller values are considered capable of finding a better diverse set of non-dominated solutions. At last, a distance-based performance index is used to detect the best combination of parameters among Pareto front solutions. This index measures the closeness of Pareto solutions to the ideal point called mean ideal distance (MID) and is calculated as follows:

$$\text{MID} = \frac{\sum_{i=1}^{m} \sqrt{\left(\frac{f_{ij} - f_i^b}{f_i^w - f_i^b}\right)^2}}{n} \quad j = 1, 2, \ldots, n \qquad (3)$$

where n is the number of generated non-dominated solutions from MOGA, m is the number of the objective function, f_{ij} is the value of jth solution of objective function i, f_i^b is the best or ideal value of objective function i and f_i^w is the worst value of objective function i subject to existing constraints. The solution that holds the lowest MID is the best one among Pareto front solutions.

5 Result and discussion

5.1 Performance evaluation of dry and HPC assisted machining

The role of HPC on average chip-tool interface temperature in turning different hardened 42CrMo4 steel at several speed-feed combinations compared to dry cut is shown in Fig. 2. It can be noticed that the increasing trend of cutting temperature (T) with the increase of cutting speed (V) -feed (f) -work-piece hardness(H) is common for both machining environments. But, T is found extensively lower in HPC-assisted machining compared to dry cut. In dry cutting conditions, the maximum T was 700 °C for the utmost V (165 m/min), f (0.16 mm) and H (56HRC). However, in the case of HPC delivery at the same machining combination, the maximum T reached 407 °C, almost two-third of dry cut. The lowest temperature (107 °C) was found in the HPC setting is green marked in Fig. 2a. The forced double jet of coolant made it possible to infiltrate into the whole cutting region. So that, the heat was eradicated rapidly from the zone and the chip-tool contact length and time were reduced. These ultimately result in a lower value of temperature.
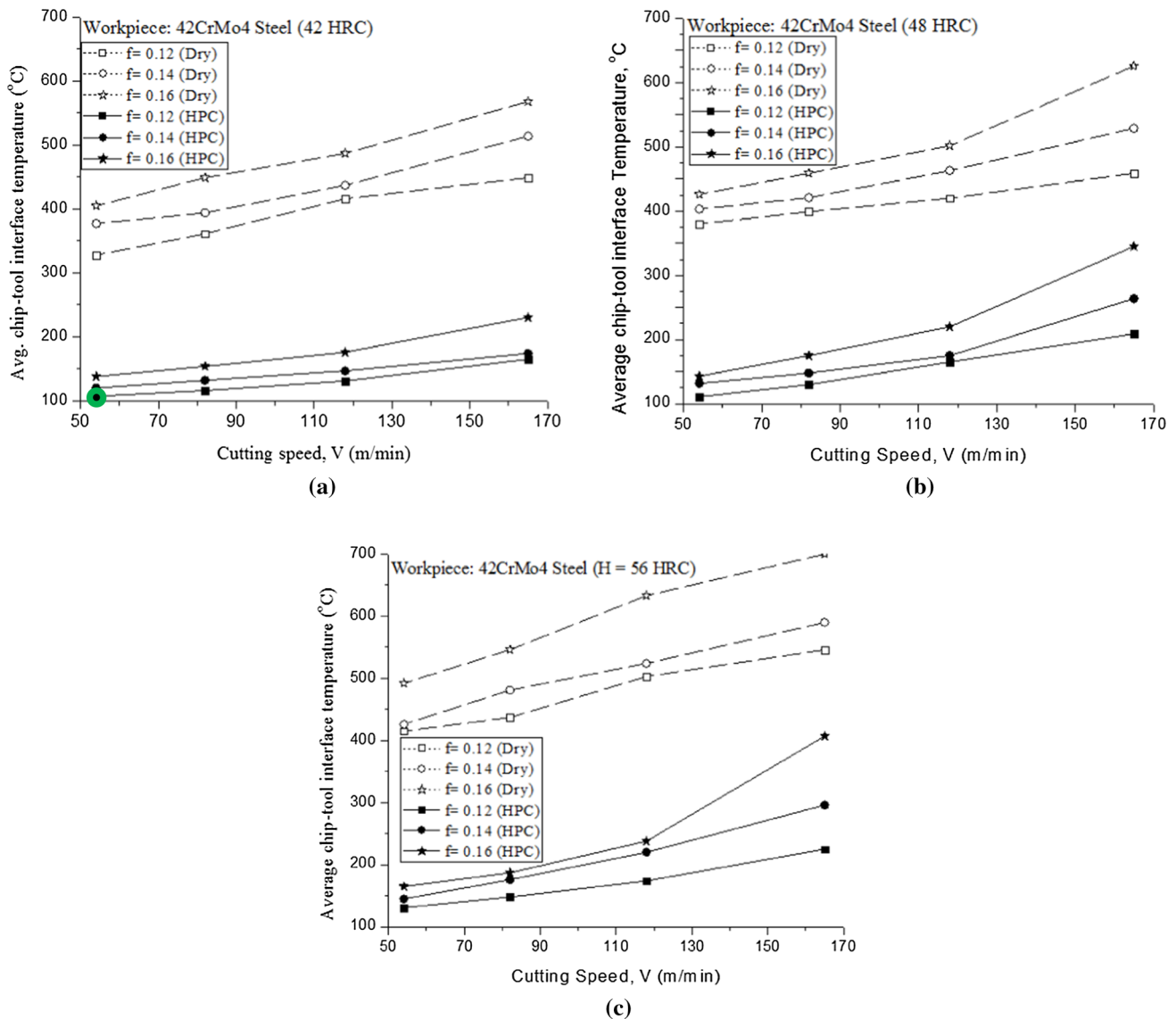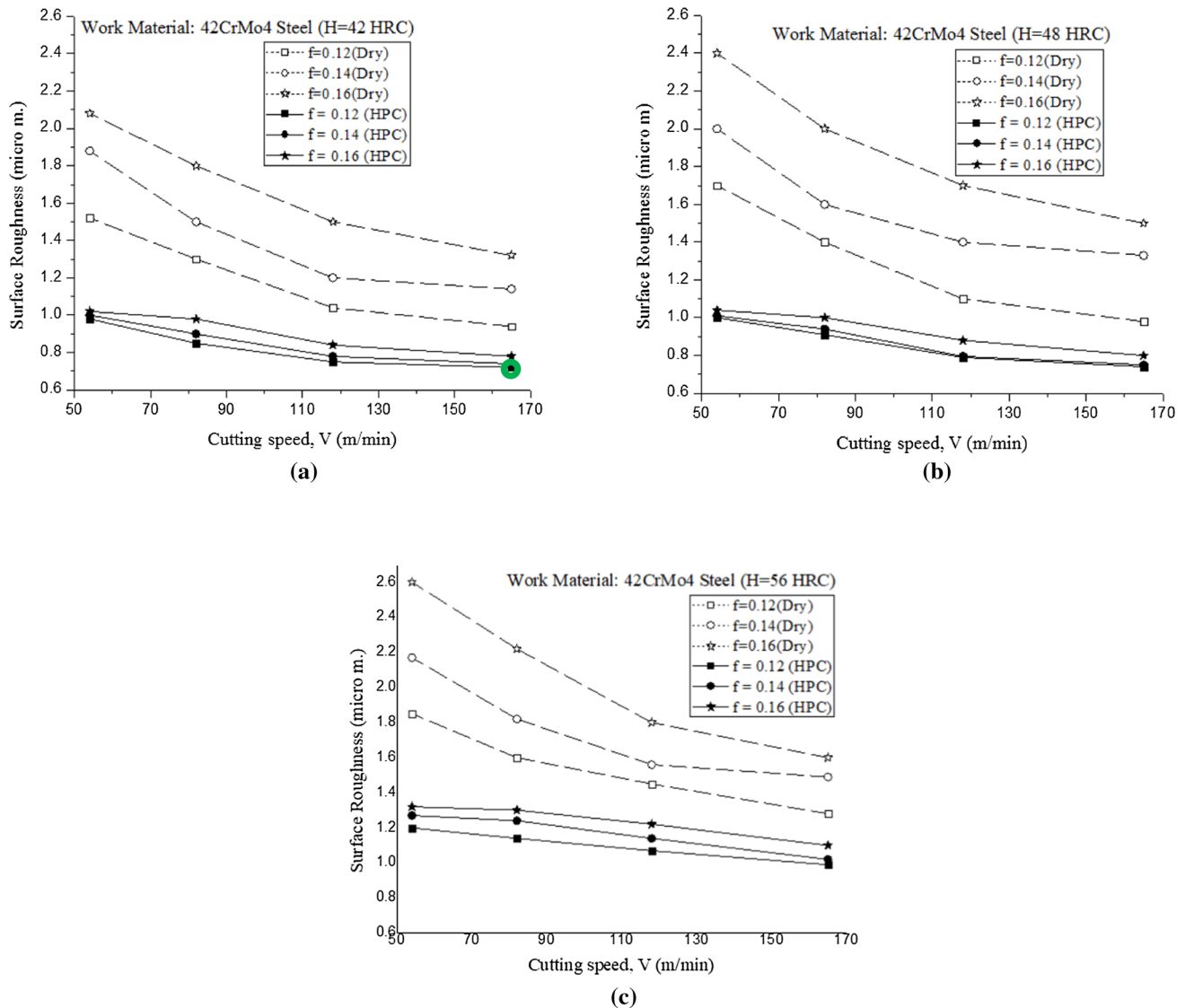
Fig. 2 Variation of cutting temperature under different cutting conditions for turning hardened 42 CrMo4 steel with hardness of **a** 42 HRC **b** 48 HRC and **c** 56 HRC

As an indicator of product quality, surface roughness was investigated to evaluate the relative role of HPC over dry cut. The value of surface roughness (R_a) attained after machining at stated speed-feed-hardness combinations under dry and HPC conditions are shown in Fig. 3. The surface finish is improved with the increase of cutting speed. On the contrary, with the increase of feed and work-piece hardness, the machined surface deteriorates. However, there is a substantial reduction of surface roughness at all of the turning operations due to HPC compared to the dry cut. The resulting maximum R_a for the dry cut was 1.6 µm while this was reduced to 1.1 µm for HPC machining. The desired lowest value of R_a (0.72 µm) results in the HPC condition shown in Fig. 3a (green marked). Therefore, the HPC jet capably assisted in lifting the chips and consequently prevent the work surface

from rubbing against the chips. This essentially drops the surface roughness value.

The decline result of T and R_a due to HPC application is illustrated in Fig. 4a–b. Figure 4a shows that in most of the cases, the reduction percentage of T was falling with the increase of V and f. For R_a, this reduction percentage (Fig. 4b) indicates an increasing trend at lower V and f in most of the runs. However, the H value does not show any specific relation for both of the responses. The highest reduction of T was found at about 71% for 48HRC work-piece machined at the lowest V and f (54 m/min–0.12 mm) condition. Besides, the lowest T percentage reduction (41.86%) was obtained at the highest V and f (165 m/min–0.16 mm) situation in turning of 56HRC steel. Another remarkable fact is that under the high-speed condition the reduction amount

Fig. 3 Variation of surface roughness under different cutting conditions for turning hardened 42CrMo4 steel with hardness of **a** 42 HRC **b** 48 HRC and **c** 56 HRC

becomes small than low speed. The reason is that, at high cutting speed, plastic contact is increased and made the jet less effective to enter into the interface. The reduction percentage of R_a was found maximum (56.67%) for the machined surface of 48HRC work-piece at low V (54 m/min) and high f (0.16 mm), condition, whereas, lowermost (22.66%) was found for 56HRC work-piece at high V (165 m/min) and low f (0.12 mm).

5.2 Effects on responses for HPC jet machining

To investigate the pattern of parametric effects and the best run setting for desired individual responses experimental data are analyzed by S/N ratio, perturbation and contour plot.

The characteristic- S/N ratio is applied here to identify the effective factors that reduce the process variability by minimizing the effects of uncontrollable (noise) factors. At the same time, the optimal level of the process factors with a higher S/N ratio for a response is also detected. In turning operation, the desired value of selected responses (T and R) is minimum. Hence, the smaller the better S/N quality characteristic is selected and can be calculated as follows:

$$S/N = -10log \frac{1}{n}\left(\sum_{i=1}^{n} y_i^2\right)$$

where y_i is the observed data at ith experiment and n is the number of experiments.
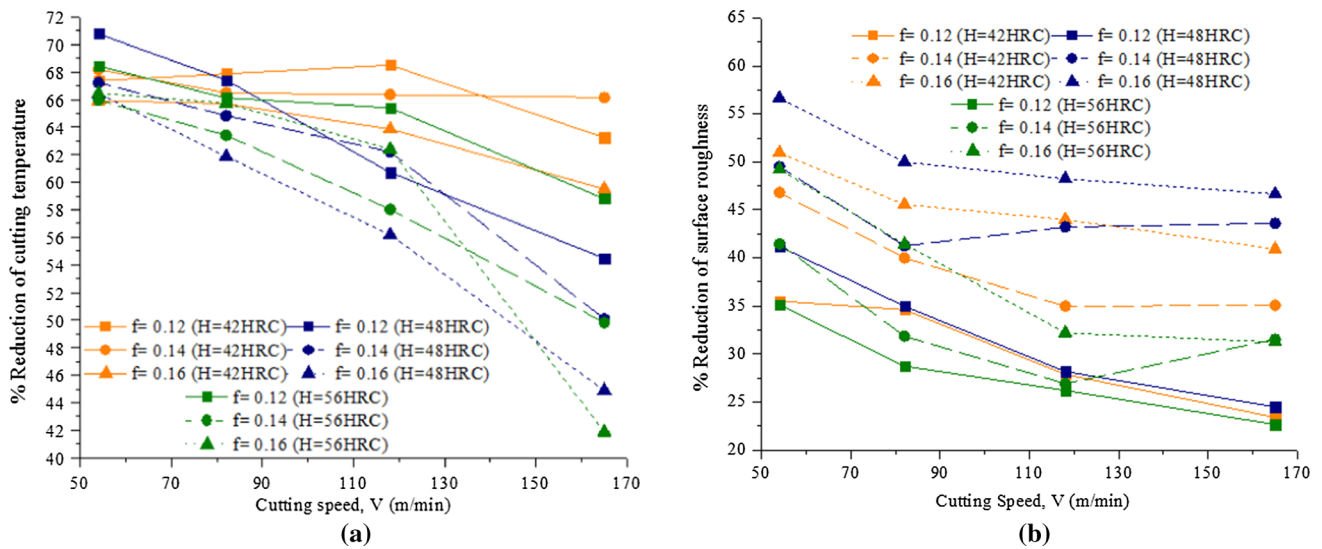
Fig. 4 HPC application effects on percent reduction of **a** Cutting temperature **b** Surface roughness

Table 3 The response for S/N ratio

	S/N ratio for T						S/N ratio for R_a					
	Level				Delta	Rank	Level				Delta	Rank
	1	2	3	4			1	2	3	4		
V	− 42.37*	− 43.53	− 45.09	− 47.85	5.48	1	− 0.72	− 0.16	0.87	1.53*	2.25	2
f	− 43.34*	− 44.64	− 46.15	--	2.80	2	0.77*	0.45	− 0.07	--	0.84	3
H	− 43.28*	− 44.88	− 45.96	--	2.68	3	1.36*	1.10	− 1.31	--	2.67	1

*Means the optimum level

Fig. 5 Main effect plot for S/N ratio of T
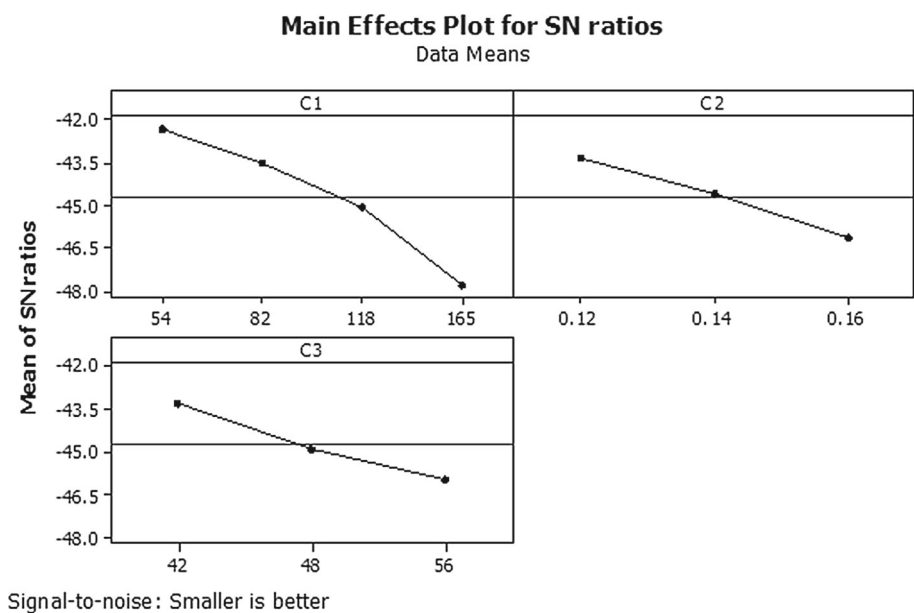
Table 3 shows the calculated S/N ratio for T and R_a at each level of the machining parameters. Based on the data presented in this table and Figs. 5 and 6 it can be inferred that the best combinations of parameters for minimizing temperature and surface roughness are $V_1 f_1 H_1$ and $V_4 f_1 H_1$, respectively. The ranking of the parameters is calculated based on the difference (delta) in the S/N ratio. The rank in Table 3 indicates the foremost parameter that affects cutting temperature is

Fig. 6 Main effect plot for S/N ratio of R_a
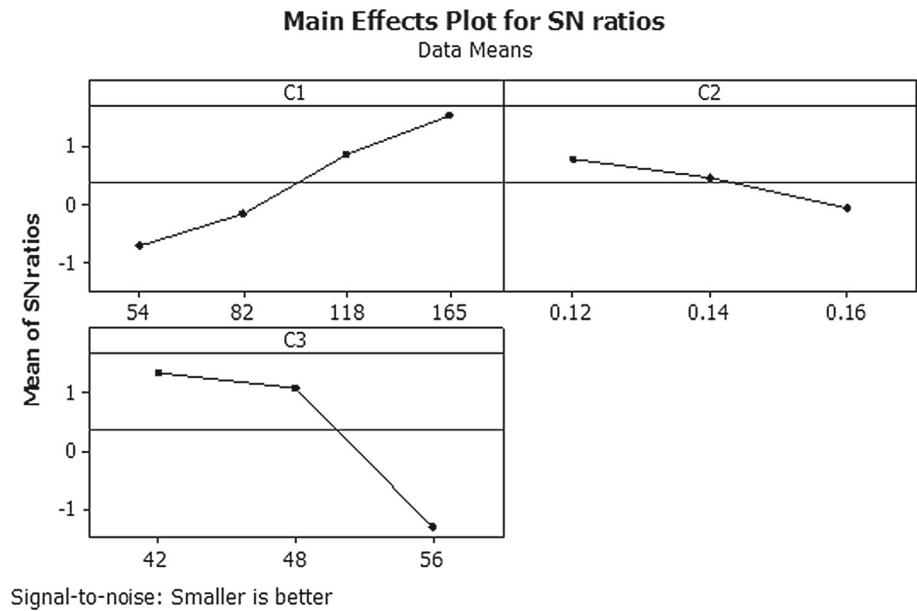
V followed by *f* and *H*. Whereas, for surface roughness, *H* ranked as the dominant parameter followed by *V* and *f*.
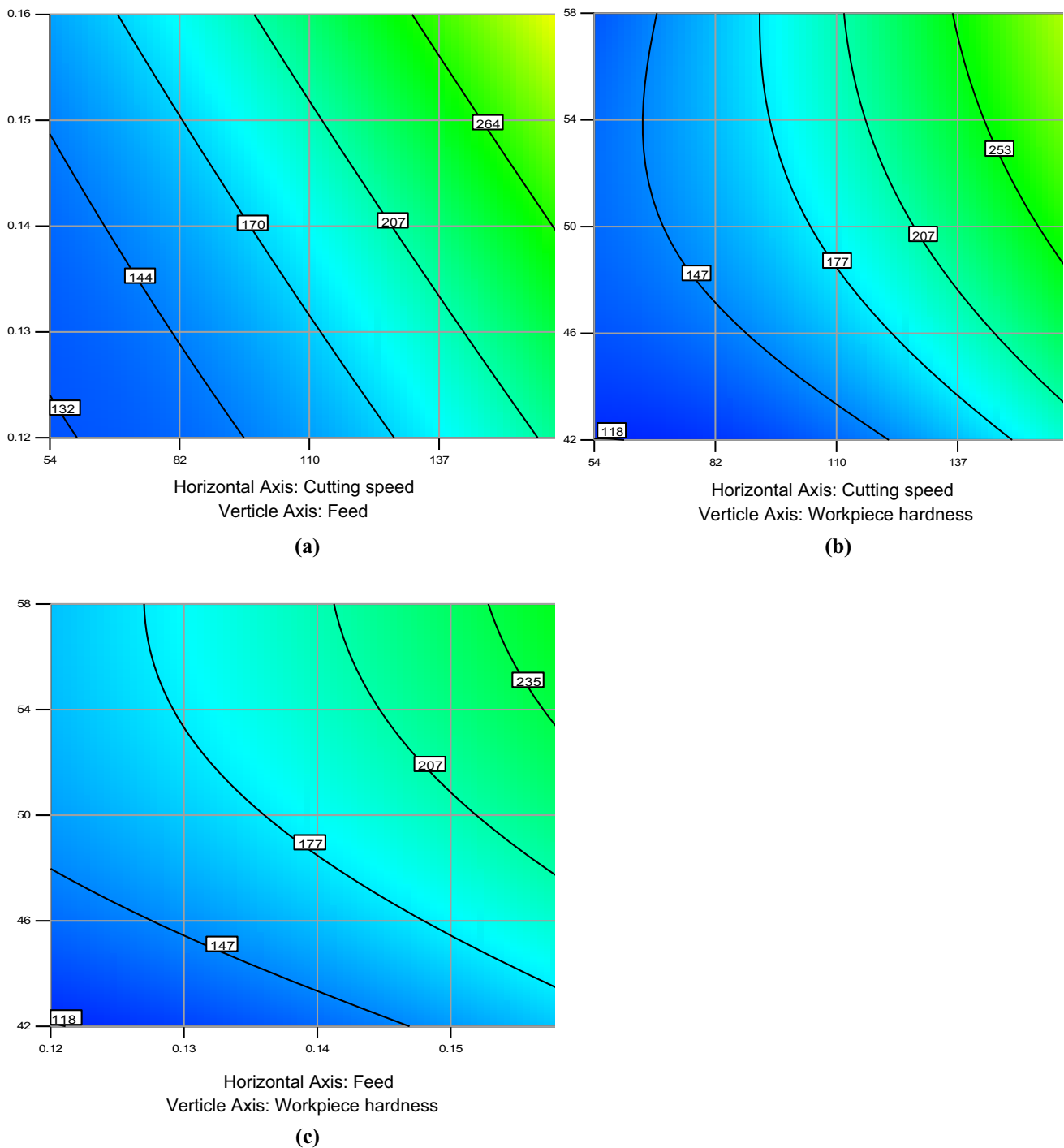
The perturbation plots of Fig. 7a–b depict the comparison of the variable effects at the center point in the design space. Here, cutting speed appeared as the most significant positive influential factor on the temperature, whereas, for surface roughness, a negative influence is observed. These figures also illustrate that feed has a secondary positive effect on both responses. In addition, work-piece hardness shows a minimal degree of positive effect on cutting temperature (Fig. 7a). Conversely, from Fig. 7b it is seen that hardness value has the most substantial positive effect on surface roughness juxtaposed to other factors. The best-run setting providing the lowest temperature (136 °C) is seen in Fig. 5a, which cor-responds to the lowest *V* (54 m/min), *f* (0.12 mm) and *H* (42HRC). From Fig. 5b the best-finshed surface (0.82 µm) is found at the highest *V* (165 m/min). Better finished surface also occur at lowest *f* (0.12 mm) and lower *H* = 43HRC. These combinations for two responses confirm the findings of the S/N ratio.

The interaction effects of parameters can be analyzed from the contour plot (Fig. 8a–c) based on the legend and color-coding. Here, the 2D plots represent a particular response for any of the two factors while the other one is constant at its mid-value (*V* = 109.50 m/min, *f* = 0.14 mm and *H* = 50HRC). The contour plots indicate the fact that all combi-nations of elevated cutting speed, higher feed, and greater work-piece hardness result in upraised cutting temperature.
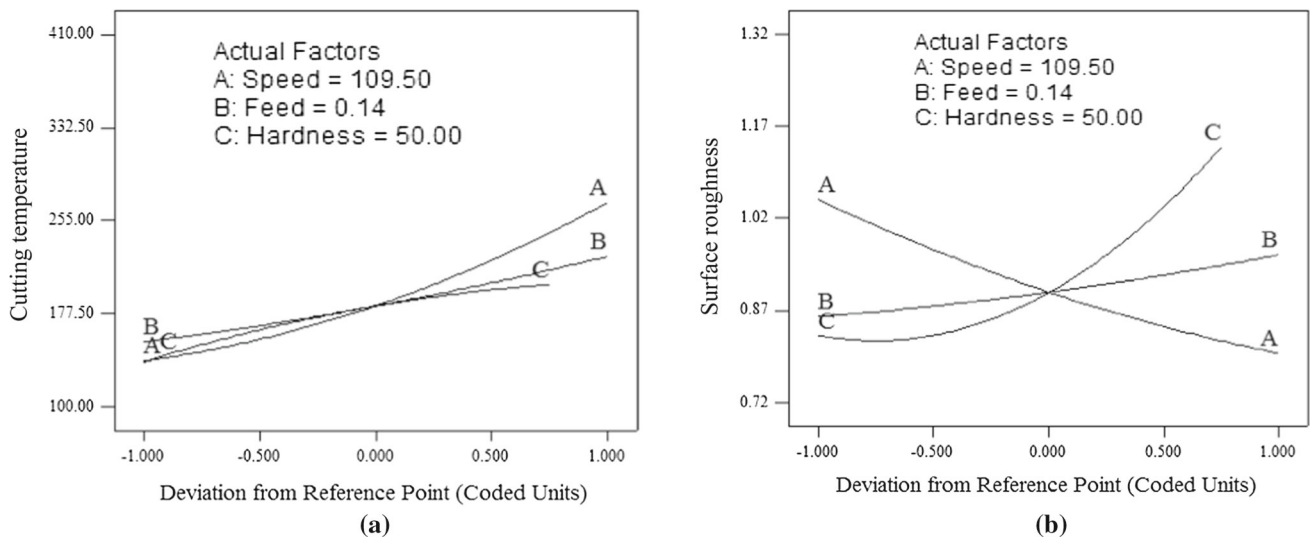
Fig. 7 Perturbation plot **a** Cutting temperature **b** Surface roughness

(a)

Horizontal Axis: Cutting speed
Verticle Axis: Feed

(b)

Horizontal Axis: Cutting speed
Verticle Axis: Workpiece hardness

(c)

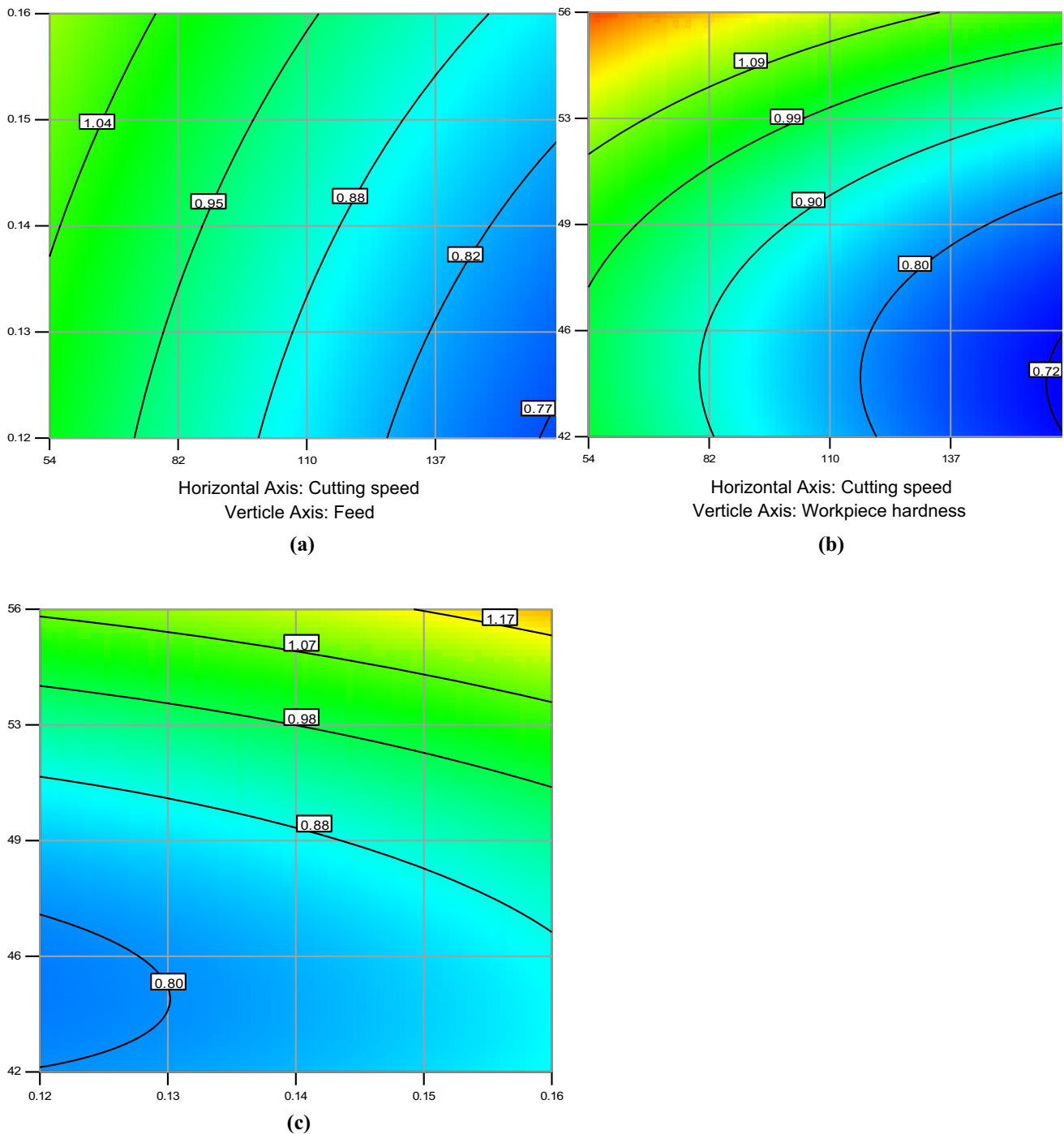Horizontal Axis: Feed
Verticle Axis: Workpiece hardness

Fig. 8 Contour plot for temperature **a** Cutting speed versus Feed **b** Cutting speed versus Work-piece hardness **c** Feed vs Work-piece hardness

That is, it is apparent that lower value (deep blue color region) of temperature occur at lower $V - f$, $V - H$ and $f - H$ combination. The least value (118 °C) comes from the lowest V (82 m/min) $- H$ (42HRC) at $f = 0.14$ mm (Fig. 8b) and from the lowest f (0.12 mm) $- H$ (42HRC) at $V = 109.50$ m/min (Fig. 8c). In the case of surface roughness desired lower value is observed at the low $f - H$ interaction (Fig. 9c), while, $V -$

f (Fig. 9a) and $V - H$ (Fig. 9b) interaction give the opposite result. That is, the better surface is found at low $f - H$; high V and low f; and at high V and low H. From Fig. 9b minimum roughness (0.72 μm) is found that takes place at the highest V (165 m/min) $-$ lowest H (42HRC) while $f = 0.14$ mm.

Therefore, cutting temperature increases with the increase of work-piece hardness level and speed-feed value. As more

Horizontal Axis: Cutting speed
Verticle Axis: Feed

(a)

Horizontal Axis: Cutting speed
Verticle Axis: Workpiece hardness

(b)

(c)

Fig. 9 Contour plot for surface roughness **a** Cutting speed versus Feed **b** Cutting speed versus Work-piece hardness **c** Feed vs Work-piece hardness

cutting speed-feed is engaged in machining, more material removal rate takes place ensues high energy consumption eventually results in the dissipation of more heat. Besides, higher cutting force generates during machining of hardened material which is also responsible for producing high temperature. Geometrically the surface roughness caused by feed marks only depends upon the value of the feed rate. That is,

with the increase in feed rate surface roughness increased at a high rate. Moreover, surface roughness is considered as a secondary level of response which mainly depends on cutting temperature and force. Machining at a higher speed, rapid cooling facilitates the thermal softening of the material, subsequently resulting in a reduced amount of cutting force. This leads to a lower surface roughness value. Furthermore,

Table 4 Sequential sum Sequential model sum of squares for cutting temperature and surface roughness

Source	Cutting temperature			Surface roughness		
	F Value	p-value > F	Remark	F Value	p-value > F	Remark
Linear versus Mean	50.91	0.000		91.10	0.000	
2FI versus Linear	14.73	0.000		0.35	0.7860	
Quadratic versus 2FI	5.17	0.006	Suggested	46.65	0.000	Suggested
Cubic versus Quadratic	10.62	0.000	Aliased	11.14	< 0.000	Aliased

Table 5 ANOVA for cutting temperature and surface roughness model

Source	df	Cutting temperature model				Surface roughness model			
		Sum of Square	Mean Square	F Value	p-value > F	Sum of Square	Mean Square	F Value	p-value > F
Model	9	1.44E5	15,939.47	64.32	0.00	1.07	0.12	179.50	0.00
V	1	82,986.52	82,986.52	334.86	0.00	0.30	0.30	449.22	0.00
f	1	28,446.53	28,446.53	114.78	0.00	0.057	0.057	85.60	0.00
H	1	17,221.07	17,221.07	69.49	0.00	0.69	0.69	1034.8	0.00
Vf	1	7441.45	7441.45	30.03	0.00	7.71E − 6	7.7E − 6	0.012	0.92
VH	1	7050.69	7050.69	28.45	0.00	6.19E − 4	6.2E − 4	0.93	0.34
fH	1	1185.47	1185.47	4.78	0.04	3.41E − 3	3.4E − 3	5.15	0.03
V^2	1	2841.16	2841.16	11.46	0.00	4.51E − 3	4.5E − 3	6.81	0.02
f^2	1	242.00	242.00	0.98	0.33	8.68E − 4	8.7E − 4	1.31	0.26
H^2	1	762.76	762.76	3.08	0.09	0.087	0.087	131.84	0.00
Residual	26	6443.50	247.83			0.017	6.6E − 4		
Corr. Total	35	1.499E5				1.09			
		R^2	Adj R^2	Pred R^2	Adeq Prec	R^2	Adj R^2	Pred R^2	Adeq Prec
		0.96	0.94	0.90	31.96	0.98	0.98	0.97	48.30

the increase of cutting speed leads smoother chip-tool interface with a minor chance of built-up-edge formation that may be attributed to a good surface finish. Particularly for harder work-piece, this surface finish deteriorated. The accelerated tool wear for the insert interaction with hard particles of materials is may be responsible for this.

5.3 RSM based modelling and optimization

5.3.1 Analysis of developed models

The experimentally measured results of cutting temperature (T) and surface roughness (R_a) from each run of HPC-oriented machining were inserted into the Design-Expert Software. At first, the selection of the not aliased highest order polynomials was performed by fit summary analysis. Additionally, other adequacy measures—adjusted R^2 and predicted R^2 with maximum values were evaluated for statistical model fitting. Consequently, the ANOVA for both response models was made to check the regression model and the significance of model terms.

The model fit summary output presented in Table 4 shows the recommendation of the quadratic model for the two responses as Probability > F is less than 0.05. The highest-order polynomial with significant additional terms was selected and the model was not aliased. Hence, it is apparent that the quadratic models are statistically fitted to the measured data.

ANOVA of each response surface model is presented in Table 5. Model terms were assessed by the F probability value with a 95% confidence level, and the significance of each coefficient was checked by the P values. The F and P values are, respectively 64.32 and < 0.00 for T and 179.50 and < 0.00 for the R model, respectively. These values indicate that the selected models are highly significant. There is only a 0.01% chance that the F values could occur due to noise. The P values of less than 0.05 imply the models as statistically significant. According to this, from Table 5 it is apparent that the main effects of cutting speed (V), feed (f), hardness (H), the interactions of $V − f$ and $V − H$, and the quadratic effect $− V^2$ are the most significant terms ($P = < 0.00$) for the T model. While, the interaction of $f − H$ is the last significant term ($P = < 0.04$) for T. Again, for the R model it can be inferred that, V, f, H and H^2 (all $P = < 0.00$) followed by V^2 ($P = < 0.02$) and $f − H$ ($P = < 0.03$) are significant terms. This table also shows the values of R^2,
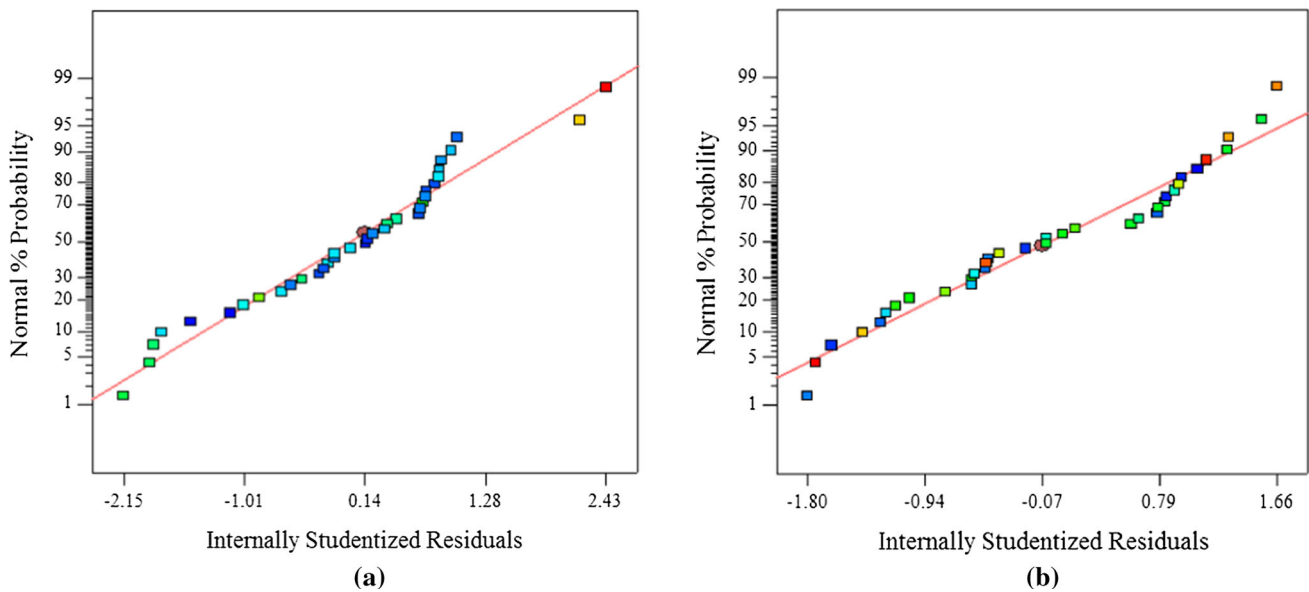
Fig. 10 Normality Test **a** Cutting temperature **b** Surface roughness

adjusted (adj.) R^2 and predicted (pred.) R^2. The R^2 value is desirable, which is close to 1 for both models (0.96 and 0.98) imply the existence of a high correlation between the model and experimental values. The adj. R^2 is 94% for T, and 98% for R_a means that the models are well fitted with the number of independent variables. Besides, for both models, pred. R^2 (0.90 and 0.97) is not that much smaller than the R^2 value directs the models' applicability in prediction for new observations which are not overfitting models. Furthermore, adequate precision ratios of T (31.96) and R_a (48.30) are well above 4 indicate adequate signals to use the models. The developed models determined by the software are given below:

$$T = 509.8971 - 6.1557V - 7456.9432f + 9.5674H$$
$$+ 21.2001Vf + 0.0588VH + 61.2753fH + 0.0066V2$$
$$+ 13750f2 - 0.2041H2 \tag{4}$$

$$R_a = 6.3609 - 0.0048V - 9.9009f - 0.2085H$$
$$- 0.0007Vf + 0.000017VH + 0.1039fH$$
$$+ 0.0000083V2 + 26.0417f2 + 0.0022H2 \tag{5}$$

5.3.2 Statistical validity test

The normal probability plots of residual values for cutting temperature and surface roughness are illustrated in Fig. 10. The experimental data points fall reasonably close to the straight line indicates the normality of data. Figure 11

shows studentized residuals versus predicted values for the responses where the residuals are scattered randomly about zero ensures constant variance of errors. It also shows that, the data points are inside $\pm 3\sigma$ limits and there is no existence of outliers. That confirms no points to give a misleading result. Figure 12 displays the interactions of the actual and predicted values of the responses showing residuals are close to the diagonal line. That is, both of the models are satisfactory as well as the predicted results are found in good agreement with the experimental data.

5.3.3 Result of RSM based optimization

Multi response optimization was carried out based on the design of experiment-RSM. The optimum values of parameters- speed (V), feed (f) and hardness (H) were attained by numerical optimization applying the desirability function with the range between 0 to 1. The goal used for the responses cutting temperature (T) and surface roughness (R_a) is "minimize" and for the parameters is "within range". In this approach, different best solutions are obtained and the combination with the highest desirability is preferred. A set of five optimal results is derived for the design space, tabulated in Table 6. The best optimum values for this process are found as $V = 147$ m/min, $f = 0.12$ mm and $H = 42$HRC at the optimal results of $T = 138$ °C and $R_a = 0.73$ μm as depicted in Fig. 13 with the utmost overall desirability of 0.9413. The dot on each ramp indicates the best solution within the given boundaries. The desirability of each parameter, response and combined values are shown in the bar graph (Fig. 14). The optimal region values holding overall desirability of 0.9413 exhibits proximity to target response.
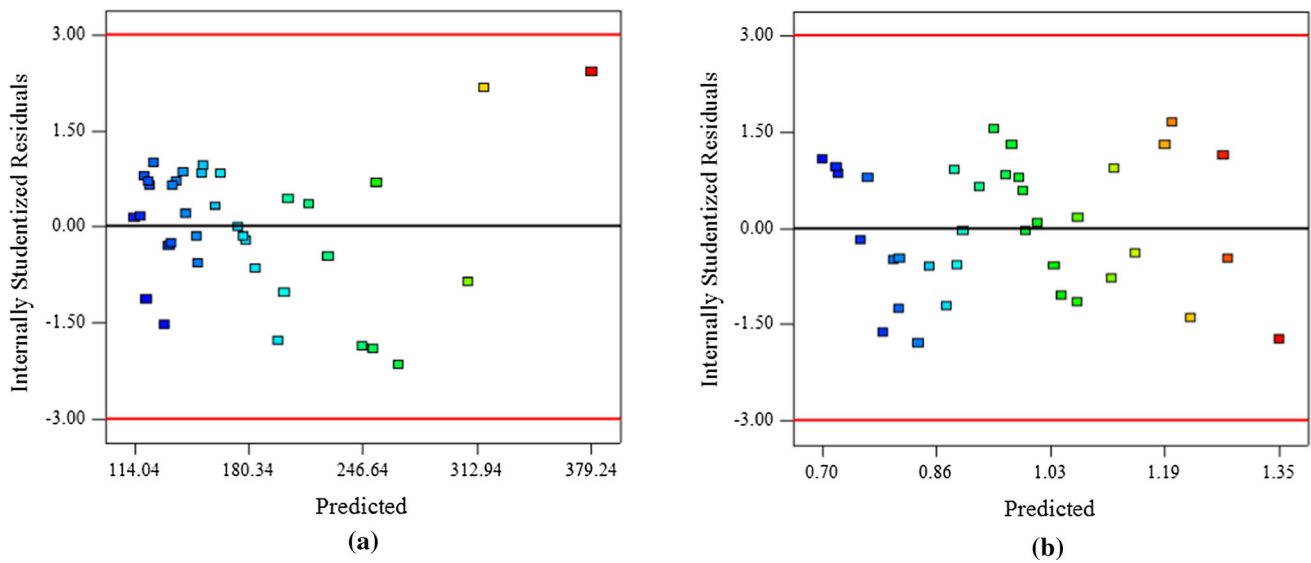
Fig. 11 Standardized residual versus predicted plot **a** Cutting temperature **b** Surface roughness
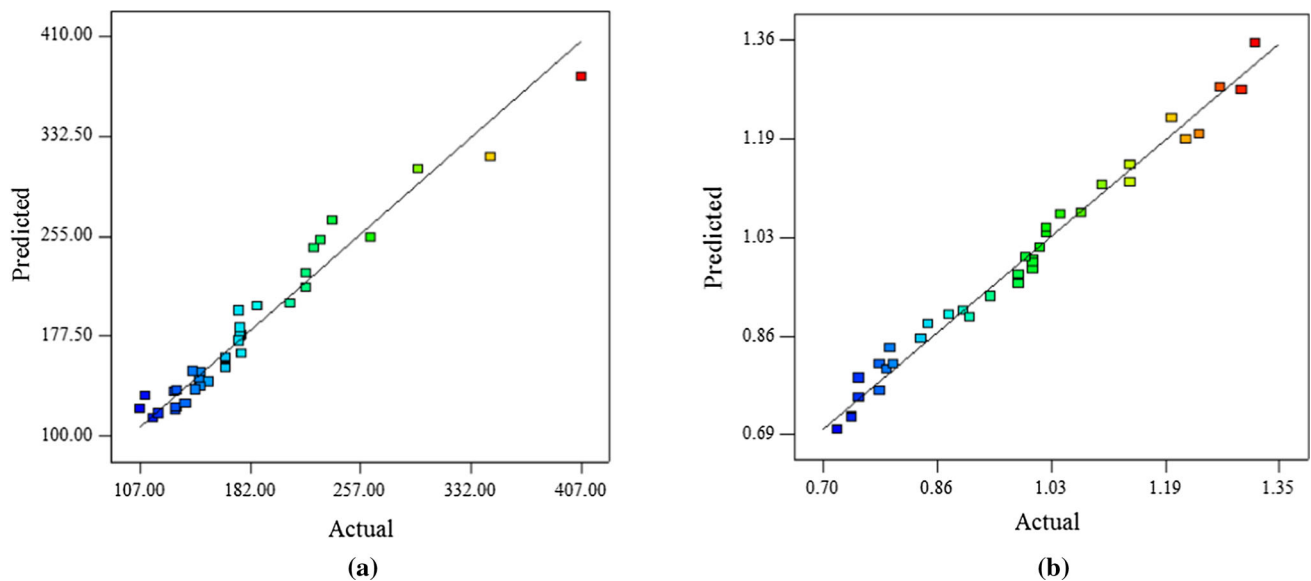

Fig. 12 Predicted vs. actual plot **a** Cutting temperature **b** Surface roughness

5.4 Analysis of GA-based optimization

The optimization problem consists of two objective functions and variable bounds. The goal function of the model was to minimize the cutting temperature and surface roughness. To optimize the multi-objective of Eqs. (4) and (5), the MOGA function 'gamultiobj' was used from the toolbox of MATLAB.

$$
\begin{aligned}
f(1) = {} & 509.8971 - 6.1557V - 7456.9432f + 9.5674H \\
& + 21.2001Vf + 0.0588VH + 61.2753fH \\
& + 0.0066V2 + 13750f2 - 0.2041H2
\end{aligned}
$$

- *Objective functions* Minimize cutting temperature, *f(1)* and surface roughness, *f(2)*.

$$
\begin{aligned}
f(2) = {} & 6.3609 - 0.0048V - 9.9009f - 0.2085H \\
& - 0.0007Vf + 0.000017VH + 0.1039fH \\
& + 0.0000083V2 + 26.0417f2 + 0.0022H2
\end{aligned}
$$

Table 6 Optimal solution from DoE based optimization

Solution no	V(m/min)	f(mm/rev.)	H(HRC)	T(°C)	R_a(µm)	Desirability
1	147	0.12	42	138	0.73	0.9413
2	145	0.12	42	136	0.73	0.9412
3	151	0.12	42	141	0.72	0.9411
4	141	0.12	42	133	0.74	0.9404
5	137	0.12	42	130	0.75	0.9388

Fig. 13 Ramp function graph
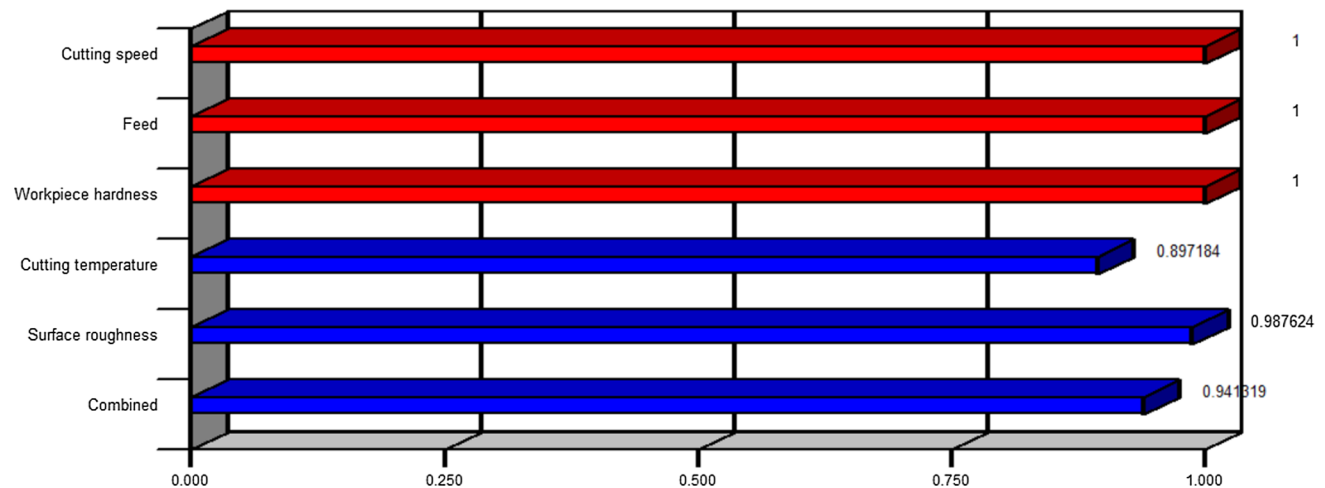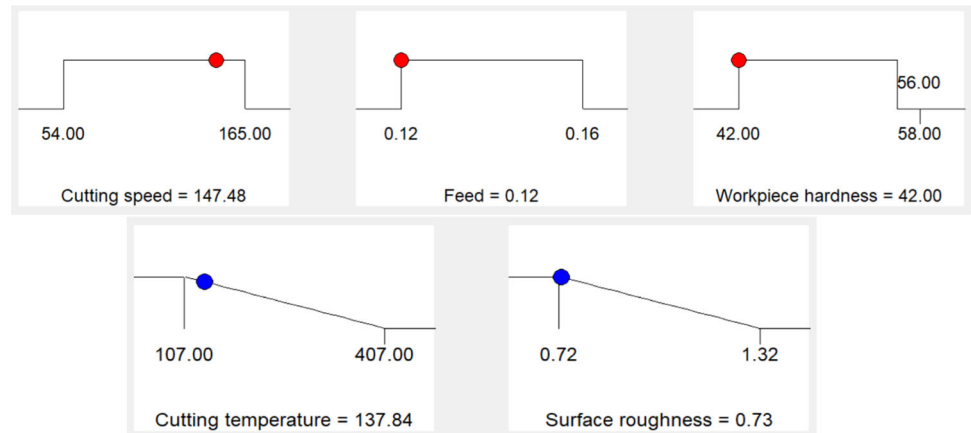
Fig. 14 Desirability bar graph

- *Decision variables* The constructed optimization model consists of three decision variables; cutting speed (V), feed (f) and work-piece hardness (H).
- *Variable bounds* Following variable bounds were selected based on the experimental parametric range of decision variables.

$$54 \le V \le 165$$
$$0.12 \le f \le 0.16$$
$$42 \le H \le 56$$

The results of performed ANOVA test to select the number of generations (n_g) are shown in Table 7. The method was planned to apply by starting with $n_g = 100$ and testing successively for every 100 until no more variation in means is observed. The variations were assessed by the F probability value with a 95% confidence level. Here, it is found and apparent from the table that there is no existence of a significant difference between n_g values of 100 and 200, since ($P > 0.05$). However, 100 difference of n_g between two runs is trivial for the GA algorithm. So, there might be a possibility of some differences for a large number. Hence, a continuation of the successive 5 test runs was carried out and up to 600 there were still no differences found for both of the responses between the compared runs. So, it can be decided that $n_g = 600$ is enough to obtain the best approximation of the present
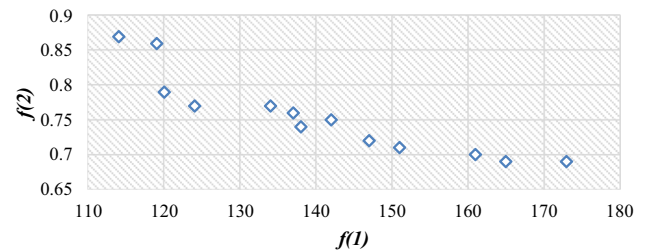
Table 7 ANOVA for cutting temperature and surface roughness model

Compared generations	Objectives	Source	Sum of squares	Mean square	F	P
$n_g = 100$ versus $n_g = 200$	f(1)	Between groups	121	121	0.29	0.59
		Within groups	14,107	415	–	–
	f(2)	Between groups	0.0004	0.0004	0.01	0.92
		Within groups	0.1345	0.0040	–	–
$n_g = 200$ versus $n_g = 300$	f(1)	Between groups	15	15	0.04	0.89
		Within groups	13,409	394	–	–
	f(2)	Between groups	0.0005	0.0005	0.14	0.71
		Within groups	0.1301	0.0038	–	–
$n_g = 300$ versus $n_g = 400$	f(1)	Between groups	42	42	0.09	0.76
		Within groups	15,334	451	–	–
	f(2)	Between groups	0.0001	0.0001	0.03	0.87
		Within groups	0.1651	0.0049	–	–
$n_g = 400$ versus $n_g = 500$	f(1)	Between groups	2	2	0.00	0.95
		Within groups	34	15,677	–	–
	f(2)	Between groups	0.0003	0.0003	0.06	0.81
		Within groups	0.1399	0.0041	–	–
$n_g = 500$ versus $n_g = 600$	f(1)	Between groups	0	0	0.00	0.98
		Within groups	15,439	454	–	–
	f(2)	Between groups	0.0006	0.0006	0.15	0.70
		Within groups	0.1344	0.0040	–	–

Table 8 MOGA generated optimal cutting parameters with MID

No. of solution	V(m/min)	f(mm/rev)	H(HRC)	f(1)	f(2)	MID
1	86	0.12	42	114	0.87	0.109
2	86	0.12	43	119	0.86	0.110
3	117	0.12	42	120	0.79	0.105
4	125	0.12	42	124	0.77	0.104
5	120	0.12	44	134	0.77	0.108
6	124	0.12	44	137	0.76	0.108
7	139	0.13	43	138	0.74	0.107
8	128	0.12	44	142	0.75	0.109
9	151	0.12	43	147	0.72	0.108
10	152	0.12	43	151	0.71	0.109
11	163	0.12	43	161	0.70	0.112
12	164	0.12	43	165	0.69	0.113
13	165	0.12	44	173	0.69	0.117

Fig. 15 Pareto front

measure of individuals about the preceding one. The value was small (0.0159) as well ensures the diversity of searching results. MID values are also included in Table 7. Followed by Eq. (3) the values are computed where $f_1^b = f_2^b = 0$ as the goal of the objectives is minimization. The combination of $V = 125$ m/min, $f = 0.12$ mm, $H = 42$HRC (solution no. 4) outperforms others in terms of MID criterion as it retains the least MID (0.104).

To compare the optimal solution set resulting from DoE and GA (Tables 6 and 8) based optimization it can be inferred that, latter procedure provides an immense range of parametric values. As it is seen, GA provides $V = 86 - 165$ m/min whereas, a reduced range of 137-151 m/min results from DoE based optimization. On the other hand, f and H is stuck to 0.12 mm and 42HRC, respectively at the solution set of DoE based optimization. But, MOGA gives two feed values – 0.12 mm and 0.13 mm and a hardness range of 42-44HRC.

Pareto front solutions. Table 8 presents the Pareto front set obtained after 186 iterations at $n_g = 600$. The solutions are ranked by cutting speed values from the lowest to the highest order. Figure 15 displays the Pareto front; the obtained non-dominated solutions, which are subjected to minimization. Figure 16 indicates the distance measure of each individual from its neighbors is 0.0165 which is small as desired. Similarly, Fig. 17 shows the average spread in the distance
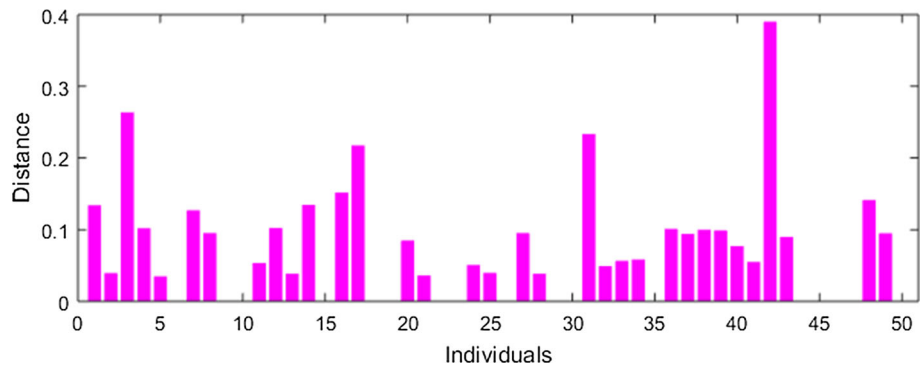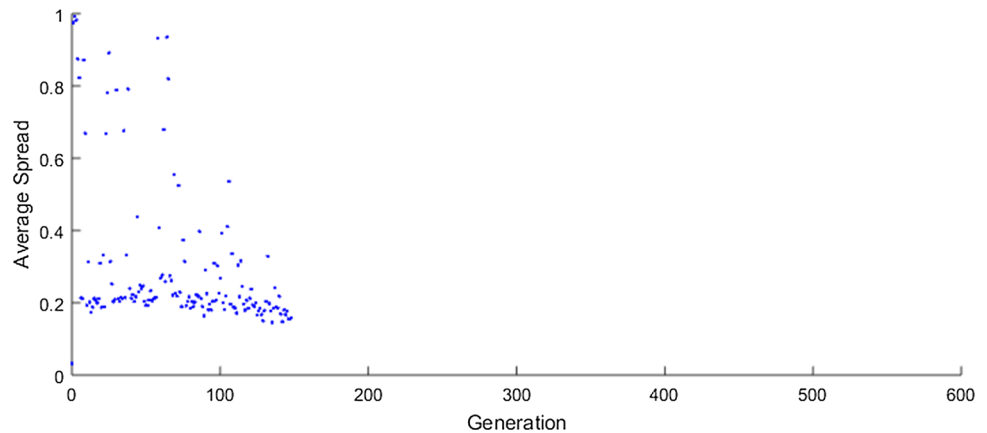
Fig. 16 Average Pareto distance plot

Fig. 17 Average Pareto spread plot

Thus, more options are available to choose from here. At the same time, compared to DoE based optimization, the lowest values of desired responses ($T = 114$ °C and $R_a = 0.69$ μm) are possible to get by following any of the respective MOGA-based combinations.

5.4.1 Confirmation experiments

From the non-dominated solution set, three runs (solution no. 1, 4, 13 of Table 8) were chosen randomly to verify the prediction of response variables. These three confirmatory experimental runs at HPC condition and the response measurements were carried out by maintaining the same machining settings stated earlier. This verification revealed a superior agreement with the predicted response values with less than 5% error (Table 9) for both of the responses. It is also notable that, for surface roughness, this error remains only within 2%.

6 Conclusion

The present research work was aimed to get the optimal cutting condition by satisfying the variable constraints of the planned experimental range of cutting speed (54–165 m/min), feed rate (0.12–0.16 mm/rev), and work-

piece hardness (42–56HRC) while turning 42CrMo4 alloy steel under HPC condition. The analysis was started with the evaluation of the effects of HPC over dry condition on the response of cutting temperature and surface roughness. Intended for HPC-assisted machining, responses' predictive models were developed and MOGA was performed concerning the stated variables to minimize both of the responses. The following points can be concluded from the study:

- At the highest speed-feed-hardness condition cutting temperature is maximum for both dry and HPC environments. However, the high-pressure coolant application facilitated the reduction of chip-tool interface temperature up to a significant level for all experimental runs compared to dry cut. The temperature percentage reduction ranges from ≈ 42 to $\approx 71\%$ with an average of 62%.
- Minimum surface roughness is attainable for lower hardened material machining with higher speed and lower feed for both cutting environments. With the application of HPC jet, obtained surface finish is much better than the situation of dry cut that was found almost 38% less than dry cut.
- Cutting speed and work-piece hardness is the most important factor influencing positively the cutting temperature and surface roughness, respectively. The only negative effect results for surface roughness possessed by cutting speed.

Table 9 Confirmation test result based on optimization

Optimal parameter values			Predicted responses		Measured responses		Error (%)	
V (m/min)	f (mm)	H (HRC)	T (°)	R_a (μm)	T (°C)	R_a (μm)	T	R_a
86	0.12	42	114	0.87	111	0.86	2.70	1.16
125	0.12	42	124	0.77	128	0.78	3.13	1.28
165	0.12	44	173	0.69	181	0.70	4.42	1.43

- The mathematical modeling by RSM provides a quadratic model for both of the responses for HPC machining. The ANOVA table also reveals that cutting speed and hardness has the greatest effect on cutting temperature and surface roughness respectively. Again, in the role of variable interaction, only cutting temperature shows significant interaction with a speed-feed combination followed by speed-hardness. Concerning the quadratic effect of variables, cutting speed exhibits a significant effect on cutting temperature whereas, for surface roughness, work-piece hardness shows the significance level.
- The R^2 value for both of the response models is greater than 95%. That is, the capability of the prediction of the model is acceptable. In addition, several statistical validity tests confirm that the predicted models are satisfactory in describing the performance indicators.
- The Pareto-based method provides non-dominated solutions to problems coupled with GA. Since none of the solutions in the Pareto optimal set is better than any other, any of the combinations is an acceptable solution that can be varied depending on the manufacturer's requirement. The solution set gives the results of input are in the range of 86 m/min to 165 m/min speed, 0.12 mm/rev to 0.13 mm/rev feed rate and HRC 42 to HRC 44 work-piece hardness. This optimal outcome set indicates that within the experimental design under HPC condition machining at the increased speed while maintaining the lower feed and work-piece hardness results in lower cutting temperature and surface roughness value.

Declarations

References

1. Senthil Kumar, A., Raja Durai, A., Sornakumar, T.: Machinability of hardened steel using alumina based ceramic cutting tools. Int. J. Refract. Metals Hard Mater. **21**(3–4), 109–117 (2003). https://doi.org/10.1016/S0263-4368(03)00004-0
2. Umbrello, D., Rizzuti, S., Outeiro, J.C., Shivpuri, R., M'Saoubi, R.: Hardness-based flow stress for numerical simulation of hard machining AISI H13 tool steel. J. Mater. Process. Technol. **199**(1–3), 64–73 (2008). https://doi.org/10.1016/j.jmatprotec.2007.08.018
3. Bogdan, A., Gavrilă, C.: The economic efficiency of replacing grinding with hard turning. Recent **18**(2), 71–76 (2017)
4. Thamizhmanii, S., Hasan, S.: Measurement of surface roughness and flank wear on hard martensitic stainless steel by CBN and PCBN cutting tools. J. Achiev. Mater. Manuf. Eng. **31**(2), 415–421 (2008)
5. List, G., Nouari, M., Géhin, D., Gomez, S., Manaud, J.P., Le Petit-corps, Y., Girot, F.: Wear behaviour of cemented carbide tools in dry machining of aluminium alloy. Wear **259**(7–12), 1177–1189 (2005). https://doi.org/10.1016/j.wear.2005.02.056
6. Totten, G.: Handbook of Residual Stress and Deformation of Steel. ASM International, Materials Park, Ohio (2002)
7. Matsumoto, Y., Barash, M.M., Liu, C.R.: Residual stress in the machined surface of hardened steel. In: High Speed Machining Conference, ASME WAM. pp.193–204. (1984)
8. Outeiro, J.C., Umbrello, D., M'Saoubi, R.: Experimental and numerical modelling of the residual stresses induced in orthogonal cutting of AISI 316L steel. Int. J. Mach. Tools Manuf. **46**(14), 1786–1794 (2006). https://doi.org/10.1016/j.ijmachtools.2005.11.013
9. Ulutan, D., Erdem Alaca, B., Lazoglu, I.: Analytical modelling of residual stresses in machining. J. Mater. Process. Technol. **183**(1), 77–87 (2007). https://doi.org/10.1016/j.jmatprotec.2006.09.032
10. Nasr, M.N.A., Ng, E.-G., Elbestawi, M.A.: A modified time-efficient FE approach for predicting machining-induced residual stresses. Finite Elem. Anal. Des. **44**(4), 149–161 (2008). https://doi.org/10.1016/j.finel.2007.11.005
11. Kramar, D., Kopač, J.: High pressure cooling in the machining of hard-to-machine materials. J. Mech. Eng. **55**(11), 685–694 (2009)
12. Kamruzzaman, M., Rahman, S.S., Ashraf, Md.Z.I., Dhar, N.R.: Modeling of chip–tool interface temperature using response surface methodology and artificial neural network in HPC-assisted turning and tool life investigation. Int. J. Adv. Manuf. Technol. **90**, 1547–1568 (2017). https://doi.org/10.1007/s00170-016-9467-6
13. Machado, A.R., Wallbank, J., Pashby, I.R., Ezugwu, E.O.: Tool performance and chip control when machining tI6Al4v and inconel 901 using high pressure coolant supply. Mach. Sci. Technol. **2**(1), 1–12 (1998). https://doi.org/10.1080/10940349808945655
14. Kaminski, J., Alvelid, B.: Temperature reduction in the cutting zone in water-jet assisted turning. J. Mater. Process. Technol. **106**(1–3), 68–73 (2000). https://doi.org/10.1016/S0924-0136(00)00640-3

15. Senthil Kumar, A., Rahman, M., Ng, S.L.: Effect of high-pressure coolant on machining performance. Int. J. Adv. Manuf. Technol. **20**(2), 83–91 (2002). https://doi.org/10.1007/s001700200128

16. Ezugwu, E.O.: Key improvements in the machining of difficult-to-cut aerospace superalloys. Int. J. Mach. Tools Manuf. **45**(12–13), 1353–1367 (2005). https://doi.org/10.1016/j.ijmachtools.2005.02.003

17. Globočki-Lakić, G., Sredanović, B., Kramar, D., Kopač, J.: Machinability of C45e steel - application of minimum quantity lubrication and high pressure jet assisted machining techniques. T FAMENA **40**(2), 45–58 (2016). https://doi.org/10.21278/TOF.40204

18. Mia, M., Khan, M.A., Dhar, N.R.: High-pressure coolant on flank and rake surfaces of tool in turning of Ti-6Al-4V: investigations on surface roughness and tool wear. Int. J. Adv. Manuf. Technol. **90**(5–8), 1825–1834 (2017). https://doi.org/10.1007/s00170-016-9512-5

19. Umbrello, D., Filice, L.: Improving surface integrity in orthogonal machining of hardened AISI 52100 steel by modeling white and dark layers formation. CIRP Ann. **58**(1), 73–76 (2009). https://doi.org/10.1016/j.cirp.2009.03.106

20. Rao, C.J., Rao, D.N., Srihari, P.: Influence of cutting parameters on cutting force and surface finish in turning operation. Procedia Eng. **64**, 1405–1415 (2013). https://doi.org/10.1016/j.proeng.2013.09.222

21. Singla, A., Singh, T.: Optimization of process parameters on CNC turning. Int. J. Curr. Eng. Technol. **6**(2), 657–661 (2016)

22. Özel, T., Karpat, Y., Figueira, L., Davim, J.P.: Modelling of surface finish and tool flank wear in turning of AISI D2 steel with ceramic wiper inserts. J. Mater. Process. Technol. **189**(1–3), 192–198 (2007). https://doi.org/10.1016/j.jmatprotec.2007.01.021

23. Suresh, R., Basavarajappa, S.: Effect of process parameters on tool wear and surface roughness during turning of hardened steel with coated ceramic tool. Procedia Mater. Sci. **5**, 1450–1459 (2014). https://doi.org/10.1016/j.mspro.2014.07.464

24. Bartarya, G., Choudhury, S.K.: Effect of cutting parameters on cutting force and surface roughness during finish hard turning AISI52100 grade steel. Procedia CIRP **1**, 651–656 (2012). https://doi.org/10.1016/j.procir.2012.05.016

25. Kant, G., Rao, V.V., Sangwan, K.S.: Predictive modeling of turning operations using response surface methodology. AMM **307**, 170–173 (2013). https://doi.org/10.4028/www.scientific.net/AMM.307.170

26. Mia, M., Dhar, N.R.: Effectof high pressure coolant jet on cutting temperature, tool wear and surface finish in turning hardened (HRC 48) steel. J. Mech. Eng. **45**(1), 1–6 (2015). https://doi.org/10.3329/jme.v45i1.24376

27. Zahia, H., Athmane, Y.M., Lakhdar, B., Tarek, M.: On the application of response surface methodology for predicting and optimizing surface roughness and cutting forces in hard turning by PVD coated insert. Int. J. Ind. Eng. Comput. **6**(2), 267–284 (2015). https://doi.org/10.5267/j.ijiec.2014.10.003

28. Veldhuizen, D.A.V., Lamont, G.B.: Multiobjective evolutionary algorithms: analyzing the state-of-the-art. Evol. Comput. **8**(2), 125–147 (2000). https://doi.org/10.1162/106365600568158

29. Amouzgar, K., Bandaru, S., Andersson, T., Ng, A.H.C.: Metamodel-based multi-objective optimization of a turning process by using finite element simulation. Eng. Optim. (2019). https://doi.org/10.1080/0305215X.2019.1639050

30. Mishra, A., Gangele, D.A.: Multi-objective optimization in turning of cylindrical bars of AISI 1045 steel through Taguchi's method and utility concept. Int. J. Sci. **12**(1), 28–36 (2013)

31. Zerti, A., Yallese, M.A., Meddour, I., Belhadi, S., Haddad, A., Mabrouki, T.: Modeling and multi-objective optimization for minimizing surface roughness, cutting force, and power, and maximizing productivity for tempered stainless steel AISI 420 in turning operations. Int. J. Adv. Manuf. Technol. **102**(1–4), 135–157 (2019). https://doi.org/10.1007/s00170-018-2984-8

32. Janahiraman, T.V., Ahmad, N.: Multi objective optimization for turning operation using hybrid extreme learning machine and multi objective genetic algorithm. IJET **7**(4.35), 876–879 (2018). https://doi.org/10.14419/ijet.v7i4.35.26273

33. Konak, A., Coit, D.W., Smith, A.E.: Multi-objective optimization using genetic algorithms: a tutorial. Reliab. Eng. Syst. Saf. **91**(9), 992–1007 (2006). https://doi.org/10.1016/j.ress.2005.11.018

34. Srinath, R.N., Tirumalaa, D., Gajjelaa, R., Das, R.: ANN and RSM approach for modelling and multi objective optimization of abrasive water jet machining process. Decis. Sci. Lett. **7**, 535–548 (2018)

35. Ameur, T.: Multi-objective particle swarm algorithm for the posterior selection of machining parameters in multi-pass turning. J King Saud Univ Eng Sci. **33**, 259–265 (2021)

36. Öztürk, O., Kalyoncu, M., Ünüvar, A.: Multi objective optimization of cutting parameters in a single pass turning operation using the bees algorithm. In: 1st International Conference on Advances in Mechanical and Mechatronics Engineering, (2018)

37. Pawar, P.J., Khalkar, M.Y.: Multi-objective optimization of wire-electric discharge machining process using multi-objective artificial bee colony algorithm. Adv. Eng. Optim. Intell. Tech. **949**, 39–46 (2020)

38. Yang, S.H., Natarajan, U.: Multi-objective optimization of cutting parameters in turning process using differential evolution and non-dominated sorting genetic algorithm-II approaches. Int. J. Adv. Manuf. Technol. **49**, 773–784 (2010)

39. Deb, K., Goel, T.: Controlled elitist non-dominated sorting algorithms for better convergence. In: Zitzler, E., Thiele, L., Deb, K., Coello Coello, C.A., Corne, D. (eds.) Evolutionary Multi-Criterion Optimization, pp. 67–81. Springer, Berlin, Heidelberg (2001)

40. Onwubolu, G.C., Kumalo, T.: Optimization of multipass turning operations with genetic algorithms. Int. J. Prod. Res. **39**(16), 3727–3745 (2001). https://doi.org/10.1080/00207540110056153

41. Quiza Sardiñas, R., Rivas Santana, M., Alfonso Brindis, E.: Genetic algorithm-based multi-objective optimization of cutting parameters in turning processes. Eng. Appl. Artif. Intell. **19**(2), 127–133 (2006). https://doi.org/10.1016/j.engappai.2005.06.007

42. Petkovic, D., Radovanovic, M.: Using genetic algorithms for optimization of turning machining process. JESR **19**(1), 47–55 (2016). https://doi.org/10.29081/jesr.v19i1.139

43. Gjelaj, A., Berisha, B., Smaili, F.: Optimization of turning process and cutting force using multiobjective genetic algorithm. Univ. J. Mech. Eng. **7**(2), 64–70 (2019)

44. Khan, A.: Effect of high pressure coolant jets in turning TI-6AL-4V alloy with specialized designed nozzle. http://lib.buet.ac.bd:8080/xmlui/handle/123456789/3763 (2015)

45. Pencheva, T., Atanassov, S.A.: Modelling of a roulette wheel selection operator in genetic algorithms using generalized nets. Bioautomation **13**(4), 257–264 (2009)

46. Wahde, M.: Biologically Inspired Optimization Methods: An Introduction. WIT Press, Southampton, UK, Boston, MA (2008)

47. Cao, Y.J., Wu, Q.H.: Teaching genetic algorithm using MATLAB. Int. J. Elect. Enging. Educ. **36**(2), 139–153 (1999)

Springer